Hindawi
Shock and Vibration
Volume 2023, Article ID 8159716, 14 pages
https://doi.org/10.1155/2023/8159716

Research Article

A New Methodology for Optimal Design of Hybrid Vibration Control Systems (MR + TMD) for Buildings under Seismic Excitation

Francisco Da Silva Brandão [1] **and Letícia Fleck Fadel Miguel** [2]

[1]*Graduate Program in Civil Engineering, Federal University of Rio Grande do Sul, Porto Alegre, Brazil*
[2]*Department of Mechanical Engineering, Graduate Program in Civil Engineering, and Graduate Program in Mechanical Engineering, Federal University of Rio Grande do Sul, Porto Alegre, Brazil*

Correspondence should be addressed to Letícia Fleck Fadel Miguel; letffm@ufrgs.br

Received 14 June 2023; Revised 2 August 2023; Accepted 16 August 2023; Published 4 September 2023

Academic Editor: Vasudevan Rajamohan

This study proposes a new methodology, based on the optimization procedure by a metaheuristic algorithm, for designing a hybrid vibration control system to mitigate the dynamic response of buildings under nonstationary artificial earthquakes (NSAEs). For illustration purposes, a 10-story shear building is studied. The hybrid control system involves the use of an MR damper (MR) and a tuned mass damper (TMD) located in different places of the structure. To describe the behavior of the MR, the modified Bouc–Wen model (MBW) was used. To calculate the damping force of the MR, the clipped optimal control associated with linear quadratic regulator (LQR), CO-LQR, was considered. The optimization was performed using the whale optimization algorithm (WOA) and seismic load generated by the Kanai–Tajimi spectrum. Different control scenarios were evaluated: MR-OFF, MR-ON, CO-LQR, STMD, and CO-LQR (MR + TMD) to determine the best control scenario that can effectively control the structure. Overall, the optimized hybrid control scenario (MR + TMD) was the only one able to adapt all story drifts to the control criterion of the consulted normative. Then, CO-LQR (MR + TMD), designed via the methodology proposed in this work, proved to be the best alternative to control the seismic response of this building.

1. Introduction

Excessive vibrations can generate critical damage to the building structure and even structural collapse, which causes economic losses and, the most serious, life losses. Regarding seismic loads, when the excitation frequencies align with the building's first natural frequencies, resonance phenomena can occur, leading to potentially catastrophic damage. In this setting, vibration control emerges as a viable alternative for mitigating these vibrations to levels deemed acceptable, according to the normative criterion adopted, as in specifications of NBR 15421 [1] used in Brazil, in NSR-10 regulation [2] adopted in Colombia, and in ANSI/AISC 360–16 [3] in the United States.

Control systems can be categorized into passive, active, semiactive, and hybrid configurations [4–6]. Concerning the semiactive system, it gathers characteristics from passive and active devices, necessitating minimal energy input to generate control forces. In hybrid systems, a blend of passive and active, or passive and semiactive devices, can be employed to regulate structural responses, thereby achieving optimal performance and yielding a highly efficient structural control [6].

One of the semiactive devices frequently utilized, which has been extensively investigated by numerous researchers over the past three decades, is the magneto-rheological damper (MR), which can generate controllable damping forces through the application of electrical current in magneto-rheological fluids (MRF). According to [7], the application of a magnetic field to MRF leads to a modification in their mechanical properties.

MR devices have found diverse applications in a range of structures and contexts. For instance, these devices have been integrated into the Dongting Lake Bridge located in China [8], incorporated within the Nihon-Kagaku-Miraikan Building situated in Japan [9], and utilized in a residential building in Japan where they were combined with a base-isolation system, resulting in a hybrid control mechanism [10]. Additionally, MR devices have been employed on the Eiland Bridge in the Netherlands [11], serving as a shock isolation system to supplant a conventional passive shock isolation system for commercial-off-the-shelf (COTS) equipment operating within demanding military tactical environments [12]. Furthermore, they have been implemented as semiactive primary suspensions for heavy trucks [13], among other varied applications.

Concerning passive devices, the tuned mass damper (TMD) stands out as one of the extensively adopted supplementary damping mechanisms. The TMD configuration comprises a mass interconnected to the system through a spring and a viscous damper [14, 15]. Within the literature, instances of TMD applications can be identified across a spectrum of structural contexts. Notable examples include its implementation in prominent structures such as the John Hancock Tower in Boston, USA; Sydney Tower in Sydney, Australia; Millennium Bridge in London, UK; and the Rio–Niterói Bridge in Brazil [16, 17].

TMD is the goal of interest of many designers and researchers such as the author of [18] who has authored a comprehensive book providing an in-depth analysis of the optimal tuning frequency of a TMD with internal damping; the authors of [19] calculated the parameters of multiple tuned mass dampers (MTMDs) arranged horizontally at the uppermost level of a ten-story building subjected to seismic excitations; the authors of [20] used a single TMD (STMD) to mitigate the dynamic response of two buildings under seismic excitations; the authors of [21] introduced a hybrid formulation featuring two distinct algorithms, namely, the firefly algorithm and the Nelder-Mead algorithm, for global optimizing of MTMDs in structures exposed to seismic excitations; the authors of [22] proposed a comprehensive study focusing on the robust optimal design of a TMD system to be installed in a tall building subjected to vibrations induced by wind forces; the authors of [23] proposed a robust optimization of MTMDs for vibration control of footbridges under human-induced vibrations. With the objective of enhancing the damping effectiveness of TMD, different configurations of the device were being developed such as vibration absorbers with linear plus cubic spring support [24], impact vibration absorbers [25], and particle-tuned mass damper [15, 26, 27].

Combining MR damper with passive devices, such as TMD, a hybrid control is generated, which can obtain excellent results as demonstrated by many researchers, for example, the work by [28] who extensively explored the semiactive control of a building complex utilizing an MR damper and TMD under earthquake excitation through numerical simulations. The authors of [28] used as a case study a building complex that includes a 14-story main building and an 8-story podium structure. The assessment of performance encompassed three distinct categories: first, the analysis of semiactive control strategies; second, the examination of hybrid semiactive control involving both the TMD and MR damper; and third, the evaluation of passive control using solely the TMD. To facilitate effective control forces, fuzzy logic was adopted to design a controller capable of determining and applying the appropriate voltage to the MR damper. The numerical findings demonstrated substantial mitigation of seismic responses in both buildings through the implementation of semiactive control and hybrid semiactive control.

In [29], the performance of a semiactive TMD with an adaptive MR damper was investigated using type-1 and type-2 fuzzy controllers for seismic vibration mitigation of an 11-degree of freedom building model. The authors of [29] explore the effectiveness of a semiactive TMD equipped with an adaptive MR damper. The study delves into the application of both type-1 and type-2 fuzzy controllers to mitigate seismic vibrations in an 11-degree-of-freedom building model. The location of the TMD was on the roof, while the MR damper was situated on the 11th story. Notably, the MR damper possessed the capability to generate a control force of 1000 kN. The design of the fuzzy system was based on the acceleration and velocity measurements of the top floor. This system determined the requisite input voltage for producing the control force based on the acceleration or deceleration movements of the building. The outcomes of the study showed that the implementation of the type-2 fuzzy controller yielded additional reductions in the maximum displacement, acceleration, and base shear of the structure, amounting to 11.7%, 14%, and 11.2%, respectively, in comparison to the results achieved with the type-1 fuzzy controller.

In [30], an investigation is presented regarding the formulation of hybrid control strategies employing three distinct combinations of MR dampers and TMDs for the purpose of regulating seismic responses in building frames. The controlled responses were derived from the analysis of four earthquakes (El Centro, Uttarkashi, Spitak, and Kobe), employing a total of four distinct control algorithms. The findings indicated that by incorporating a combination of TMD and a reduced number of MR dampers, a noteworthy enhancement in control response of up to 40%–45% could be achieved.

When optimization is used to design the vibration control systems, its efficiency can be further improved. Regarding the optimized design of passive systems based on the TMD, in [31], the application of the differential evolution (DE) algorithm is discussed with regard to designing optimal parameters for a tuned impact damper (TID), which draws inspiration from the TMD. According to [31], this design process is rooted in the utilization of an equivalent reduced-order model, and it uses the TID attached to a 20-story nonlinear benchmark building. As main conclusions, the authors highlight the possibility of using the reduced-order model for large and complex engineering structures; significantly mitigating the dynamic response of the principal structure–notably, in terms of peak displacement, RMS displacement, and interstory drift ratio–through the integration of an optimized TID system; evidencing a notable

reduction in the occurrence of plastic hinges by virtue of the optimized TID system, and the optimized TID system exhibits remarkable robustness, and a validation corroborated by its proficient performance in dynamically responding to a large number of earthquake records affecting the main structure.

In [32], the application of an MR damper is explored to enhance the operational efficiency of a benchmark base-isolated building. The MR damper is strategically positioned between the structure's base and the foundation. The optimization of MR damper parameters is executed through the utilization of the particle swarm optimization (PSO) algorithm, employing a suite of benchmark earthquake records. The outcomes of the study demonstrated a notable improvement in the dynamic response under all soil conditions, as contrasted with scenarios involving non-optimized configurations and base isolation. Furthermore, the efficacy of the optimization process in enhancing the response of base-isolated structures was well-established.

In [33], an exploration is conducted on a hybrid control system that combines an MR damper and a TMD. The investigation is carried out using a 15-story shear building as the experimental context. Specifically, the MR damper is affixed to the TMD structure, enabling it to generate an active control force for the TMD mechanism. The control voltage for the MR damper is generated through the integration of two distinct control algorithms. These algorithms are optimized using the observer-teacher-learner-based optimization (OTLBO) algorithm and aimed to minimize the maximum displacement of the building's rooftop. This optimization process is conducted under the influence of both far-field and near-field earthquake excitations. The findings revealed a substantial average reduction of 35.06% in building rooftop displacement achieved through the implementation of the fractional-order proportional-integral-derivative (FOPID) control system, coupled with the interval type-2 fuzzy logic controller (IT2FLC). This reduction was observed across sixteen distinct far-field and near-field earthquake records. Furthermore, it was established that the hybrid system (MR + TMD), outperformed conventional controllers, underscoring its superior efficacy in seismic response mitigation.

In this context, this study presents a novel methodology for designing a hybrid control system. This system involves the utilization of a magnetorheological (MR) damper and a tuned mass damper (TMD) positioned at distinct locations within the structure. The ultimate goal is to mitigate the structural response of a 10-story shear building when subjected to seismic loads, specifically a nonstationary artificial earthquake (NSAE) generated by the Kanai–Tajimi spectrum [34, 35]. To execute the optimization process, the study harnesses the power of the whale optimization algorithm (WOA). Developed by the authors of [36], this metaheuristic algorithm mimics the hunting behavior of humpback whales.

2. Mathematical Model of the Dynamic Problem

To describe the dynamic behavior of multiple degrees of freedom (n-DOF) system, with linear behavior, subjected to seismic excitation and control forces generated by a semi-active or hybrid vibration control system, which in this study is MR + TMD, the following differential equation of motion is employed:

$$\mathbf{M_s}\ddot{\mathbf{x}}(t) + \mathbf{C_s}\dot{\mathbf{x}}(t) + \mathbf{K_s}\mathbf{x}(t) = -\mathbf{M_s}\Lambda\ddot{\mathbf{x}}_{\mathbf{g}}(t) - \Gamma\mathbf{f_{mr}}(t), \tag{1}$$

in which $\mathbf{M_s}$, $\mathbf{C_s}$, and $\mathbf{K_s}$ represent the structure global matrices of mass, damping, and stiffness, respectively. $\ddot{\mathbf{x}}(t)$, $\dot{\mathbf{x}}(t)$, and $\mathbf{x}(t)$ are, respectively, the acceleration, velocity, and displacement vectors. The seismic and control force vectors are given by the term on the right of equation (1), where Λ is the location vector of the seismic forces, which is associated with the vector of seismic accelerations, $\ddot{\mathbf{x}}_{\mathbf{g}}(t)$. Finally, Γ is the control force location matrix of the control force vector, $\mathbf{f_{mr}}(t)$. And using the state-space (SS) formulation to solve this problem, and considering an n-DOF system with m MR actuators, equation (1) can be rewritten as follows:

$$\dot{\mathbf{x}}(t)_{(2nx1)} = \mathbf{A}_{(2nx2n)}\mathbf{x}(t)_{(2nx1)} + \mathbf{B_c}_{(2nxm)}\mathbf{f_{mr}}(t)_{(mx1)} + \mathbf{E}_{(2nx1)}\ddot{\mathbf{x}}_{\mathbf{g}}(t), \tag{2}$$

$$\mathbf{y}(t)_{(3nx1)} = \mathbf{C}_{(3nx2n)}\mathbf{x}(t)_{(3nx1)} + \mathbf{D_c}_{(3nxm)}\mathbf{f_{mr}}(t)_{(mx1)} + \mathbf{F}_{(3nx1)}\ddot{\mathbf{x}}_{\mathbf{g}}(t), \tag{3}$$

in which $\mathbf{A}$ is a square matrix that represents the state or characteristics of the system; $\mathbf{B_c}$ describes the position of the vector control forces ($\mathbf{f_{mr}}(t)$) in the system; $\mathbf{E}$ locates the seismic acceleration vector ($\ddot{\mathbf{x}}_{\mathbf{g}}(t)$); $\mathbf{C}$ is a square matrix and represents the output matrix; and $\mathbf{D_c}$ and $\mathbf{F}$ describe the positions of the vectors of control forces and seismic accelerations, respectively. Considering the equation of the vector of states, $\dot{\mathbf{x}}_{(2nx1)}$, the equations that govern each term of its equation are as follows:

$$\begin{aligned}
\mathbf{A}_{(2nx2n)} &= \begin{bmatrix} \mathbf{0}_{(nxn)} & \mathbf{Id}_{(nxn)} \\ -\mathbf{M_s}^{-1}\mathbf{K_s}_{(nxn)} & -\mathbf{M_s}^{-1}\mathbf{C_s}_{(nxn)} \end{bmatrix}, \\
\mathbf{B}_{(2nxm)} &= \begin{bmatrix} \mathbf{0}_{(nxm)} \\ -\mathbf{M_s}^{-1}\Gamma_{(nxm)} \end{bmatrix}, \\
\mathbf{f_{mr}}(t)_{(mx1)} &= \{f_1, f_2, f_3, \ldots, f_m\}^{\mathrm{T}}, \\
\mathbf{E}_{(2nx1)} &= \begin{bmatrix} \mathbf{0}_{(nx1)} \\ -\Lambda_{(nx1)} \end{bmatrix}.
\end{aligned} \tag{4}$$

And, to the output vector, $\mathbf{y}(t)_{(3nx1)}$, the equations are as follows:

$$\mathbf{C}_{(3nx2n)} = \begin{bmatrix} \mathbf{Id}_{(nxn)} & \mathbf{0}_{(nxn)} \\ \mathbf{0}_{(nxn)} & \mathbf{Id}_{(nxn)} \\ -\mathbf{M_s}^{-1}\mathbf{K}_{s\,(nxn)} & -\mathbf{M_s}^{-1}\mathbf{C}_{s\,(nxn)} \end{bmatrix},$$
$$\mathbf{D}_{c\,(3nxm)} = \begin{bmatrix} \mathbf{0}_{(2nxm)} \\ -\mathbf{M_s}^{-1}\Gamma_{(nxm)} \end{bmatrix}, \quad (5)$$
$$\mathbf{F}_{(3nx1)} = \begin{bmatrix} \mathbf{0}_{(2nx1)} \\ -\Lambda_{(nx1)} \end{bmatrix}.$$

Rewriting equations (2) and (3) and considering that:

$$\mathbf{B}_{ce\,(2nxm+1)} = \left[\mathbf{B}_{(2nxm)}\mathbf{E}_{(2nx1)}\right];\ \mathbf{u}(t)_{(m+1x1)} = \begin{Bmatrix} \mathbf{f}_{mr}(t) \\ \ddot{\mathbf{x}}_{g}(t) \end{Bmatrix},$$
$$\mathbf{D}_{ce\,(3nxm+1)} = \left[\mathbf{D}_{c\,(3nxm)}\mathbf{F}_{(3nx1)}\right];\ \mathbf{u}(t)_{(m+1x1)} = \begin{Bmatrix} \mathbf{f}_{mr}(t) \\ \ddot{\mathbf{x}}_{g}(t) \end{Bmatrix}. \quad (6)$$

Finally, it arrives at the SS equation of the n-DOF system subjected to control forces and seismic excitation, as represented in equation (1):

$$\dot{\mathbf{x}}(t)_{(2nx1)} = \mathbf{A}_{(2nx2n)}\mathbf{x}(t)_{(2nx1)} + \mathbf{B}_{ce\,(2nxm+1)}\mathbf{u}(t)_{(m+1x1)}, \quad (7)$$

$$\mathbf{y}(t)_{(3nx1)} = \mathbf{C}_{(3nx2n)}\mathbf{x}(t)_{(3nx1)} + \mathbf{D}_{ce\,(3nxm+1)}\mathbf{u}(t)_{(m+1x1)}, \quad (8)$$

in which $\mathbf{B_{ce}}$ and $\mathbf{D_{ce}}$ are the location matrices of the control and excitation forces, respectively. It should be noted that, when a passive control system through TMD or multiple TMDs to generate a hybrid control (MR + TMD) is added to the system, the global matrices of the structure ($\mathbf{M_s}$, $\mathbf{C_s}$, and $\mathbf{K_s}$) are modified to consider the influence of these passive devices. In equations (7) and (8), n is the number DOF, and m is the number of MR actuators.

3. Methodology

3.1. Seismic Excitation. In conducting the dynamic analysis of the examined building within this study, a nonstationary artificial earthquake (NSAE) was employed. This earthquake record was specifically generated using the Kanai–Tajimi spectrum [34, 35]. The model's equation is defined through a power spectral density (PSD) function denoted as $S(\omega)$, as presented in equation (9). Within this equation, S_0 represents the constant spectral density, while ξ_g and ω_g denote the soil damping and frequency, respectively. The soil damping was specified as $\xi_g = 0.6$ a type of rocky soil, obtained from [37], and to the soil frequency, a value of $\omega_g = 4\pi$, which is an intermediate value between the first and second mode of vibration of the building under analysis, was employed.

$$S(\omega) = S_0\left[\frac{{\omega_g}^4 + 4{\omega_g}^2{\xi_g}^2\omega^2}{\left(\omega^2 - {\omega_g}^2\right)^2 + 4{\omega_g}^2{\xi_g}^2\omega^2}\right] \text{ with}$$
$$S_0 = \frac{0,03\xi_g}{\pi\omega_g\left(4{\xi_g}^2 + 1\right)}. \quad (9)$$

Equation (9) delineates a function within the frequency domain. To facilitate its transition into the time domain, the utilization of equation (10), developed by [38], was adopted. Within this equation, $\Delta\omega$ denotes the frequency increment, N_ω signifies the interval number of band frequencies, and φ_j corresponds to the random phase angle. The values of φ_j are uniformly distributed over the range from 0 to 2π.

$$\vec{\ddot{\mathbf{u}}}_{\mathbf{g}}(t) = \sqrt{2}\sum_{j=1}^{N_\omega}\sqrt{S\left(\omega_j\right)\Delta\omega}\cos\ \left(\omega_j t + \varphi_j\right). \quad (10)$$

Finally, aiming to simulate the nonstationarity of the earthquakes, an envelope function (equation (11)) adapted from [39] was applied to multiply the stationary accelerogram, resulting in the generation of a new record exhibiting analogous behavior to real earthquakes. The initial parameters that governed this process were adjusted to $a_1 = 1.35\ \mathrm{s}^{-1}$ and $a_2 = 1/2\ \mathrm{s}^{-1}$. Figure 1 shows the generated NSAE and its PSD.

$$g(t) = a_1 t\exp\left(-a_2 t\right). \quad (11)$$

The peak ground acceleration (PGA) of the NSAE was specified as 0.3 g, and its duration was set to 10 s with a time step of 0.002 s.

3.2. Analyzed Building and MR Damper Modeling. The analyzed structure in this study is a 10-story shear building adapted from [19], which has one DOF per story and linear behavior. The mass, stiffness, and damping are uniform for each story whose adapted values are $m_i = 3.5\times10^4$ kg, $k_i = 6.5\times10^7$ N/m, and $c_i = 6.0\times10^5$ N·s/m, respectively. The height of each story was defined as 3.0 m. The ten natural frequencies, obtained using eigenvalues and eigenvectors formulation, are 1.0251 Hz; 3.0524 Hz; 5.0115 Hz; 6.8587 Hz; 8.5527 Hz; 10.0556 Hz; 11.3339 Hz; 12.3590 Hz; 13.1080 Hz; 13.5642 Hz.

In the literature, many numerical models able to describe the behavior of the MR damper can be found, and among them, the modified Bouc–Wen model (MBW), proposed by [40] and illustrated in Figure 2, was employed in this study.

According to [40], the Bouc–Wen model effectively forecasts the force-displacement characteristics of the damper, displaying a force-velocity behavior that aligns more closely with experimental data. Nevertheless, akin to the Bingham model, the Bouc–Wen model does not exhibit a roll-off in its nonlinear force-velocity response within the realm where acceleration and velocity exhibit opposing signs, and velocity magnitudes remain modest. To enhance the predictive capabilities of the damper's response within this specific context, a modified variant of the model was

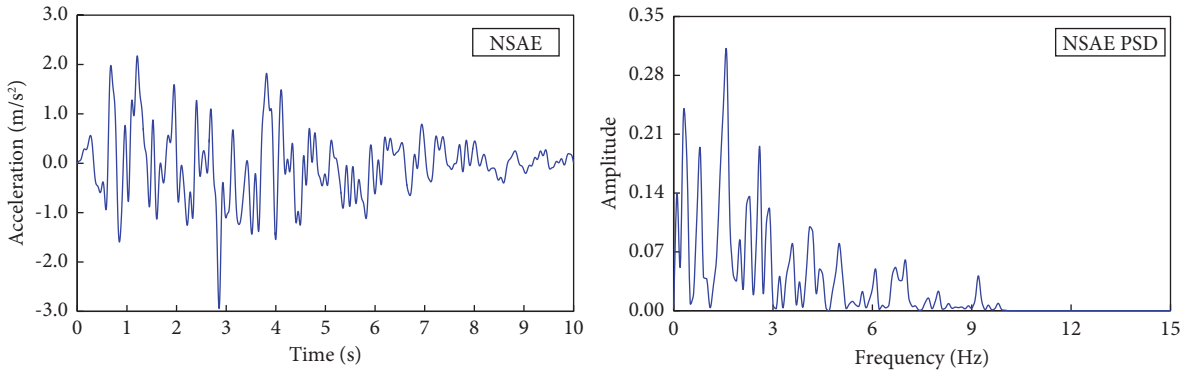

Figure 1: Nonstationary artificial earthquake (NSAE) and its PSD.

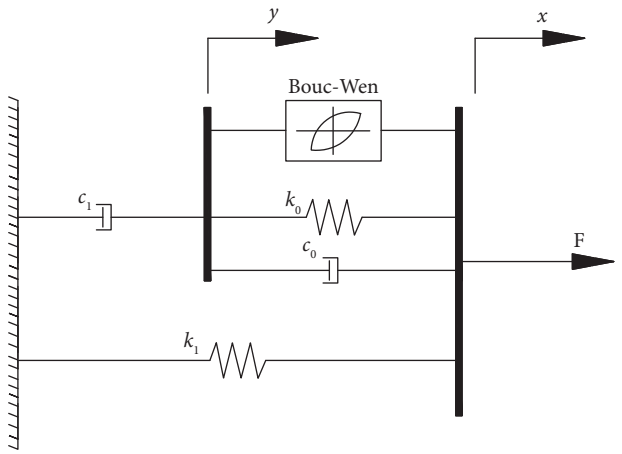

Figure 2: The modified Bouc–Wen model used to characterize the MR damper (adapted from [40]).

introduced, denoted as MBW. The damping force ($F = f_{mr}$) of this model is as follows:

$$f_{mr} = c_1\dot{y} + k_1(x - x_0), \tag{12}$$

where solving for derivative internal displacement, $\dot{y}$, results in

$$\dot{y} = \frac{1}{c_0 + c_1}\left[\alpha z + c_0\dot{x} + k_0(x - y)\right], \tag{13}$$

and, where the evolutionary variable, z, is governed by

$$\dot{z} = -\gamma|\dot{x} - \dot{y}|z|z|^{n_{bw}-1} - \beta(\dot{x} - \dot{y})|z|^{n_{bw}} + A_{bw}(\dot{x} - \dot{y}). \tag{14}$$

The terms that remain to be defined in equations (12)–(14), according to [40], are k_1 which signifies the accumulator stiffness; c_0 which represents the viscous damping observed at higher velocities; c_1 which incorporates a dashpot component aimed at introducing the roll-off phenomenon evident in experimental data at lower velocities; k_0 which is utilized to govern stiffness at elevated velocities; x_0 which designates the initial displacement associated with spring k_1 a contribution to the nominal damper force linked with the accumulator; x and $\dot{x}$ which denote the displacement and velocity, respectively, of the controlled structure; and the parameters α, β, γ, A_{bw}, and n_{bw} which describe the hysteresis of the system that depends on the physical characteristics of each MR damper, such as MR fluid, numerical model, and piston rest position. In the context of semiactive control, the building under study is subject to control through a single MR damper. This MR damper is located between the ground and the first story of the building, as shown in Figure 3(a). The MR damper was placed in this position due to the possible high value of the story drift for this story (usually, the first story has higher values) and easy installation in real life. Furthermore, once the MR damper is placed in this location, it puts a large amount of damping force on this story, which has effects on the other stories of the building. The MR used in the analyses was proposed by the authors of [41], and it is a large-scale device with a maximum damping force of approximately 200,000 N (20 tons) and a maximum operating current of 2.0 A.

According to [41], the MR damper has an internal diameter of 20.3 cm with electromagnetic coils connected in three sections of the piston, which results in four effective regions of the valve. The full device has approximately 1 m in length, mass of 250 kg, and contains approximately 6 liters of MR fluid. The MBW model parameters were obtained experimentally by the authors of [41], and some of these (α, c_0, and c_1) depend on the input current. The obtained values, as well as their equations, are shown in Table 1.

3.3. Control Law. To calculate the damping force generated by the MR damper which is applied to the structure under analysis, the clipped optimal control technique developed by the authors of [42–44] is employed. According to [8], the clipped optimal control is an optimal control strategy that has already been implemented in many civil engineering applications. The control law of this technique is based on the linear state feedback controllers, designed for active or semiactive systems, whose desired control signal is calculated using a linear controller, such as linear quadratic Gaussian (LQG) or linear quadratic regulator (LQR), combined with a clipped algorithm to limit the actuation signal to the achievable working range of the control device. In this study, the LQR combined with clipped optimal control, named here as CO-LQR, is employed to obtain the

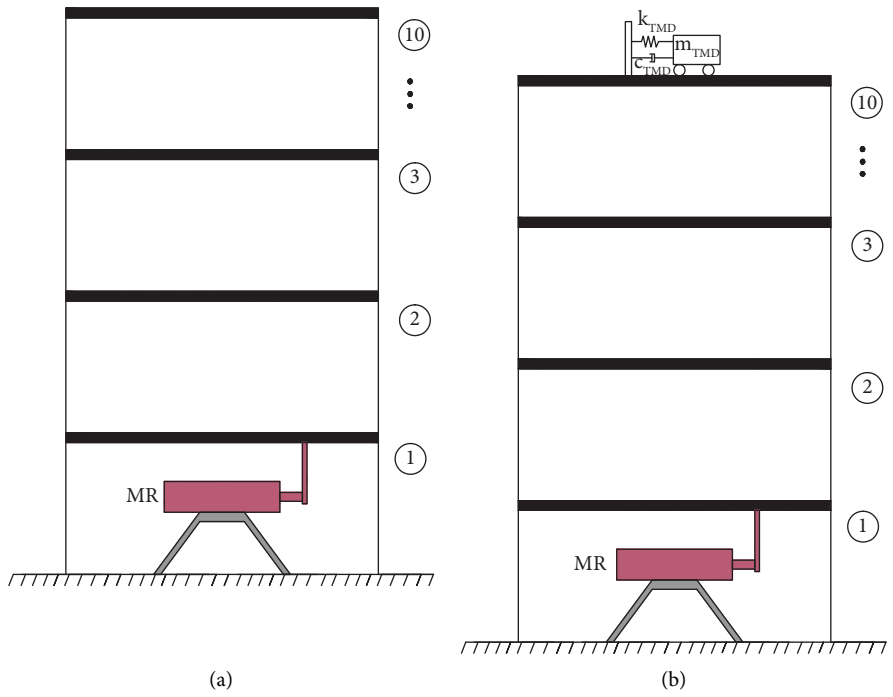

Figure 3: Vibration control of the 10-story building: (a) semiactive control and (b) hybrid control (MR + TMD).

Table 1: Parameters of the MBW model for the MR damper of 20 tons (adapted from [41]).

Current independent parameters	A_{bw} (m^{-1})	β (m^{-1})	γ (m^{-1})	k_0 (N/m)	k_1 (N/m)	x_0 (m)	n_{bw}
	2679	647.46	647.46	137810	617.31	0.18	10
Current dependent parameters	$\alpha(I) = 16566I^3 - 87071I^2 + 168326I + 15114$						
	$c_0 = 437097I^3 - 1545407I^2 + 164137I + 457741$						
	$c_1 = -9363108I^3 + 5334183I^2 + 48788640I - 2791630$						

command electric current of the MR damper, through the control law written in the following equation:

$$I_c = I_{\max} H[(f_o - f_{mr}) f_{mr}], \tag{15}$$

in which $I_{\max}$, I_c, f_o, f_{mr}, and $H(-)$ are the maximum current, the MR damper command current, the optimal control force generated by the LQR, the MR force, and the Heaviside function, respectively. To better understand this algorithm, equation (16) shows the Heaviside function, where the values of 0 or 1 depend on the comparison between the force generated by the MR and the desired optimal force.

$$H(-) = \begin{cases} 1, & \text{if } \quad |f_o| - |f_{mr}| > 0 \text{ and } f_o \cdot f_{mr} > 0, \\ 0, & \text{if } f_{mr} \cdot f_o < 0. \end{cases} \tag{16}$$

As per equation (16), when the device is exerting the desired optimal force ($f_o = f_{mr}$), the command current is maintained unchanged. If the magnitude of the force generated by the MR damper is smaller than the magnitude of the desired optimal force and the two forces share the same sign, the applied current is heightened to its maximum level. This adjustment aims to amplify the force produced by the MR damper to align with the intended control force. Conversely, when the two forces exhibit differing signs, the Heaviside function yields a value of zero. In such instances, the command current is set to zero, reflecting this condition where forces are dissimilar. Thus, to calculate the vector of control forces, $\mathbf{f_o}(t)$, generated by the LQR controller, the following equation is used:

$$\mathbf{f_o}(t) = -\mathbf{G}\mathbf{x}(t), \tag{17}$$

in which $\mathbf{x}(t)$ represents the state vector of the system with n displacements, $x(t)$, and n velocities, $\dot{x}(t)$. n is the number DOF, and $\mathbf{G}$ indicates the gain matrix, calculated using the following equation:

$$\mathbf{G} = \mathbf{R}^{-1}\mathbf{B}_\mathbf{c}^T\mathbf{P}, \tag{18}$$

in which $\mathbf{P}$ is the positive-definite symmetric matrix, which is the solution of the Riccati equation defined as follows:

$$\mathbf{A}^T\mathbf{P} + \mathbf{P}\mathbf{A} - \mathbf{P}\mathbf{B}_\mathbf{c}\mathbf{R}^{-1}\mathbf{B}^T\mathbf{P} + \mathbf{Q} = 0, \tag{19}$$

where $\mathbf{A}$ represents the system state matrix, $\mathbf{B_c}$ is the input matrix characterizing the positions of the control forces and for the LQR, and $\mathbf{Q}$ and $\mathbf{R}$ are its weighting matrices.

3.4. Proposed Hybrid Control. The hybrid control (MR + TMD) of the studied building was generated by the MR damper associated with the TMD which, according to [14, 45], consists of a mass, an elastic spring, and a viscous (or hysteretic) damper. For this system, many control scenarios are proposed, and the TMD parameters, stiffness (k_{TMD}), damping coefficients (c_{TMD}), and the weighting matrices of the LQR controller are optimized. The mass of the TMD (m_{TMD}) was chosen as 1% of the building's total mass and is not optimized.

An illustration of the hybrid control is shown in Figure 3(b) where the MR damper is positioned between the ground and the first story, and the TMD is positioned at the top floor. In Figure 3(a), only the MR is used as semiactive control to control the response for comparison purposes with the hybrid control.

The installation of the TMD at the top floor of the building requires modifications in the global matrices of mass ($\mathbf{M_s}$), stiffness ($\mathbf{K_s}$), and damping ($\mathbf{C_s}$) of the structure to incorporate the influence of the properties of the device. Therefore, equations (20)–(22) show these modifications:

$$\mathbf{M_s} = \begin{bmatrix} m_1 & 0 & \cdots & 0 & 0 \\ 0 & m_2 & \cdots & 0 & 0 \\ \vdots & \vdots & \ddots & \vdots & \vdots \\ 0 & 0 & \cdots & m_n & 0 \\ 0 & 0 & \cdots & 0 & m_{\mathrm{TMD}} \end{bmatrix}, \tag{20}$$

$$\mathbf{K_s} = \begin{bmatrix} k_1 + k_2 & -k_2 & \cdots & 0 & 0 \\ -k_2 & k_2 + k_3 & \cdots & 0 & 0 \\ \vdots & \vdots & \ddots & \vdots & \vdots \\ 0 & 0 & \cdots & k_n + k_{\mathrm{TMD}} & -k_{\mathrm{TMD}} \\ 0 & 0 & \cdots & -k_{\mathrm{TMD}} & k_{\mathrm{TMD}} \end{bmatrix}, \tag{21}$$

$$\mathbf{C_s} = \begin{bmatrix} c_1 + c_2 & -c_2 & \cdots & 0 & 0 \\ -c_2 & c_2 + c_3 & \cdots & 0 & 0 \\ \vdots & \vdots & \ddots & \vdots & \vdots \\ 0 & 0 & \cdots & c_n + c_{\mathrm{TMD}} & -c_{\mathrm{TMD}} \\ 0 & 0 & \cdots & -c_{\mathrm{TMD}} & c_{\mathrm{TMD}} \end{bmatrix}. \tag{22}$$

3.5. Story Drift Control Criterion. In this study, the response of the examined building under earthquake loading is evaluated using the concept of story drift. The story drift quantifies the disparity in horizontal displacements between two successive stories. The formula defining story drift, denoted by equation (23), involves the maximum calculated value for story drift ($\Delta_{h,\max}$), time to time. In this equation, d_i represents the displacement of the upper story, and d_{i-1} signifies the displacement of the lower story.

$$\Delta_{h,\max} = d_i - d_{i-1}. \tag{23}$$

The control criterion $h_i/400$ of each story height, in which h_i is the ith height of the ith story, was employed in the analyses. This criterion is presented in the ANSI/AISC 360–16 code of the American Institute of Steel Construction [3] and was also employed by many authors such as the authors of [46–52].

3.6. Optimization Algorithm. The whale optimization algorithm (WOA), a metaheuristic algorithm that mimics the hunting behavior of humpback whales, proposed by the authors of [36], was employed to conduct the optimization processes. In the hybrid vibration control system, both the TMD parameters and the weighting matrices of the LQR controller were simultaneously optimized. The pseudocode of WOA is shown in Figure 4 in which the parameters A and C are coefficient vectors of the leader position vector and updated positions vector. The vector a is used to calculate A, and it is linearly decreased from 2 to 0 over the course of iterations (in both exploration and exploitation phases). The parameters A, C, and a belong to the mechanism encircling prey. The parameter l is a random number in [−1, 1] and belongs to the spiral updating position equation. Finally, according to [36], the behavior of humpback whales involves a dual approach: they circle their prey within a diminishing circle while concurrently following a spiral-shaped trajectory. To mimic this simultaneous behavior, the authors adopt a 50% probability of choosing between the shrinking encircling mechanism and the spiral model to update the whales' positions. This probability, denoted as p, is governed by a random number in the range of [0, 1]. The parameters l and p are intricately linked to the bubble-net attacking method, indicative of the exploitation phase within the algorithm. Further information about the mathematical formulation and details about the three operations of WOA (encircling prey, bubble-net attacking, and search for prey) can be found by the authors of [36].

Recent applications of optimization utilizing the whale optimization algorithm (WOA) are documented in [49–51], where investigations encompassed the optimization of design parameters and placements of single TMD and multiple TMDs. These studies sought to enhance vibration control in buildings subjected to seismic excitations, with the primary objective of diminishing story drift. Furthermore, the authors of [52] conducted optimization of TMD parameters for a building under seismic loading. Additionally, the authors of [53] focused on optimizing the parameters of MTMDs to minimize the maximum vertical displacement of road bridges subjected to vehicle traffic.

4. Results and Discussions

4.1. Uncontrolled Response. Once the structure has been modeled and the seismic excitation generated, the uncontrolled response scenario (URS) of the building is evaluated. Considering that all stories of the building have the same height, defined as 3.0 m, and the story drift evaluation criterion presented in the ANSI/AISC 360–16 [3] indicates, $h_i/400$, the results obtained are presented in Table 2.

By analyzing Table 2, it can be seen that the first five stories have story drift higher than the maximum allowed according to the adopted control criterion. Therefore, based on the results, it was verified that a vibration control system

```
Initialize the whale population (Xi, where i=1, 2, 3,…, n)
Calculate the fitness of each search agent
Determine the best search agent (X*)
while (i< maximum iteration number)
    for each search agent, update the parameters a, A, C, l and p
        if1 (p<0.5)
            if2 (|A|<1)
                Update the position of the current search agent
            else if2 (|A|≥1)
                Select a random search agent (Xrand)
                Update the position of the current search agent
            end if2
        else if1 (p≥0.5)
            Update the position of the current search agent
        end if1
    end for
    Check if any search agent goes beyond the search space and amend it
    Calculate the fitness of search agent
    Update X* if there is a better solution
    i=i+1
end while
Return X*
```

Figure 4: Pseudocode of the whale optimization algorithm (WOA) (adapted from [36]).

Table 2: Maximum values of story drift for the uncontrolled response of the building subjected to the NSAE.

Story	h_i (m)	Limit of Δ_h (m)	$\Delta_{h,\max}$ for URS (m)
1	3.0	0.0075	0.0116
2	3.0	0.0075	0.0110
3	3.0	0.0075	0.0102
4	3.0	0.0075	0.0093
5	3.0	0.0075	0.0084
6	3.0	0.0075	0.0072
7	3.0	0.0075	0.0059
8	3.0	0.0075	0.0046
9	3.0	0.0075	0.0032
10	3.0	0.0075	0.0017

is necessary for this building in order to adapt it to the consulted code.

4.2. Semiactive Control Response. The first proposed scenario for the building is the semiactive with one MR damper installed between the ground and the first story (as shown in Figure 3(a)). The device is modeled based on the MBW, and it can operate in different modes: passive OFF/ON (MR-OFF and MR-ON) and semiactive with current control through the CO-LQR algorithm (CO-LQR). The MR damper used was proposed by the authors of [41] and has a maximum operating current of 2.0 A. The MBW model parameters were obtained experimentally by the authors of [41] and are shown in Table 1. For the CO-LQR scenario, **Q** was defined based on equation (24), and **R** was adjusted to $\mathbf{R} = 10^{-14}$.

$$\mathbf{Q} = \begin{bmatrix} \mathbf{K_{s(nxn)}} & \mathbf{0_{(nxn)}} \\ \mathbf{0_{(nxn)}} & \mathbf{M_{s(nxn)}} \end{bmatrix}. \tag{24}$$

The peak of the damping forces for the MR damper operating as MR-OFF, MR-ON, and CO-LQR modes was $f_{mr,\mathrm{OFF}} = 52048.5390\,\mathrm{N}$, $f_{mr,\mathrm{ON}} = 199004.9413\,\mathrm{N}$, and $f_{mr,\mathrm{CO-LQR}} = 199470.5023\,\mathrm{N}$, respectively.

4.3. Optimized Hybrid Control Response. The response of the analyzed structure is evaluated considering an optimized hybrid control system (MR + TMD) through the WOA. For comparison between the proposed hybrid control and other solutions (as semiactive control in the previous section), another control scenario, based on the passive control, is proposed. In this way, for the optimization procedure, two control scenarios are proposed, namely,

(1) STMD: single optimized TMD installed at the top floor of the building

(2) CO-LQR (MR + TMD): optimized TMD at the top of the building combined with the MR damper installed between the ground and the first story (as shown in Figure 3(b)), controlled by the optimized CO-LQR algorithm

For the STMD scenario, the TMD has mass (m_{TMD}) corresponding to 1% of the total mass of the structure, and its design parameters are optimized, namely, stiffness coefficient (k_{TMD}) and damping coefficient (c_{TMD}). The

optimization problem is expressed by equation (26), where $\Delta_{h,\max}$ represents the maximum story drift, which is the objective function of the optimization problem. The design variables are k_{TMD} and c_{TMD}, and the lower bound and the upper bound of the stiffness and damping constants of the TMD are 0–4000 kN/m and 0–1000 kNs/m, respectively.

$$\text{Find: } \mathbf{g} = \left[k_{\mathrm{TMD}}, c_{\mathrm{TMD}}\right], \tag{25}$$

$$\text{Minimizes: } f(\mathbf{g}) = \Delta_{h,\max}\ (g), \tag{26}$$

$$\text{Subject to: } \begin{cases} k_{\mathrm{TMD}}^{\min} \le k_{\mathrm{TMD}} \le k_{\mathrm{TMD}}^{\max}, \\ c_{\mathrm{TMD}}^{\min} \le c_{\mathrm{TMD}} \le c_{\mathrm{TMD}}^{\max}. \end{cases} \tag{27}$$

The results obtained for the STMD were $m_{\mathrm{TMD}} = 3500$ kg, $k_{\mathrm{TMD}} = 138734$ N/m, and $c = 469$ Ns/m, where it can be seen that the TMD tunes close to the first vibration mode of the building, with a frequency equal to $f_{\mathrm{TMD}} = 1.0020$ Hz.

For the second scenario, CO-LQR (MR + TMD), the TMD again has a mass of 1% of the structure mass, and it is installed at the top floor of the building, and its design parameters are also optimized. Furthermore, the LQR parameters (q_{LQR} and r_{LQR}) of the weighting matrices are also optimized. The objective function is the same as in equation (26), which is the minimization of the maximum story drift. The lower bound and upper bound of the stiffness and damping constants of the TMD are 0–4000 kN/m and 0–1000 kNs/m, respectively, and for the LQR are 10^{-6}–10^{18} for q_{LQR} and 10^{-20}–10^{10} for r_{LQR}. The weighting matrices were defined as $\mathbf{Q} = q_{\mathrm{LQR}}\mathrm{diag}(\mathbf{K_s}; \mathbf{M_s})$ and $\mathbf{R} = r_{\mathrm{LQR}}\,\mathbf{Id}_{(\mathbf{mxm})}$, where m is the number of MR. The maximum current of the MR is 2.0 A. Equation (29) shows the optimization problem of this control scenario.

$$\text{Find: } \mathbf{g} = \left[k_{\mathrm{TMD}}, c_{\mathrm{TMD}}, q_{\mathrm{LQR}}, r_{\mathrm{LQR}}\right], \tag{28}$$

$$\text{Minimizes: } f(\mathbf{g}) = \Delta_{h,\max}\ (g), \tag{29}$$

$$\text{Subject to: } \begin{cases} k_{\mathrm{TMD}}^{\min} \le k_{\mathrm{TMD}} \le k_{\mathrm{TMD}}^{\max}, \\ c_{\mathrm{TMD}}^{\min} \le c_{\mathrm{TMD}} \le c_{\mathrm{TMD}}^{\max}, \\ q_{\mathrm{LQR}}^{\min} \le q_{\mathrm{LQR}} \le q_{\mathrm{LQR}}^{\max}, \\ r_{\mathrm{LQR}}^{\min} \le r_{\mathrm{LQR}} \le r_{\mathrm{LQR}}^{\max}. \end{cases} \tag{30}$$

The results obtained for this control scenario were $m_{\mathrm{TMD}} = 3500$ kg, $k_{\mathrm{TMD}} = 1.6906 \times 10^5$ N/m, $c = 5.1553 \times 10^3$ Ns/m, $q_{\mathrm{LQR}} = 7.3135 \times 10^{15}$, and $r_{\mathrm{LQR}} = 1.3133 \times 10^5$. For the MR force, a value of $f_{mr,\mathrm{MR+TMD}} = 199159.2176$ N was obtained, and for the TMD, it was verified that it tunes to $f_{\mathrm{TMD}} = 1.1061$ Hz, again close to the first vibration mode of the building.

4.4. Assessment of the Responses. In the semiactive control, three approaches were initially evaluated, namely, MR damper in passive mode OFF (MR-OFF); MR damper in passive mode ON (MR-ON); and clipped optimal control with LQR (CO-LQR). In MR-OFF, the current has a constant value of 0 A, while in MR-ON, its value is 2.0 A. In CO-LQR, there is control of the applied value of the current which varies from 0 A to 2.0 A. Finally, regarding the optimized hybrid control, first, the response reduction was evaluated using an optimized STMD and, after, the CO-LQR (MR + TMD) scenario.

The response, in terms of displacements on the 10th story, is shown in Figure 5, where it can be seen that the MR-ON and CO-LQR (MR + TMD) scenarios show good reductions, especially between the 6 s and 10 s of the seismic excitation. Regarding the MR-OFF scenario, it is possible to see lower reductions, especially at the end seconds of the earthquake.

Figure 5 also shows that the STMD scenario generates an increase in the responses in terms of story drift on the last two stories, as also shown in Figure 6, which shows the story drift for each story, and in Table 3, which shows the story drift reduction percentages for all scenarios. The negative reductions of the last two stories for the STMD scenario indicate increases in the response, and it is related to the presence of the TMD in the building, because it tunes a different mode than the most excited by the earthquake, or it is related to the low mass in relation to the mass of the structure.

Figure 6, as previously mentioned, shows the maximum story drift for each story, considering all control scenarios and the limit of the consulted normative. As can be seen in Figure 6, for the URS, the first five stories have story drift higher than the maximum allowed. It is also verified that the semiactive control in modes MR-OFF, MR-ON, and CO-LQR, failed to adapt all the story drifts to the established criterion. The STMD scenario presents reasonable reductions, fitting the 4th and 5th stories to the normative criterion; however, the last two stories show increases in the response. For CO-LQR (MR + TMD), it can be seen that it was the only one able to effectively control the structural response and adapt all stories to the control criterion.

Considering the percentages of reductions for all scenarios as shown in Table 3, it is verified that the highest reduction (44.8276%) happens with the MR-ON mode at the 1st story, which has constant current applied by the MR, and the damping force is directly applied to this story. The CO-LQR (MR + TMD) also presents good reductions, and it was the only one that had effective control of the structural response. Finally, Figure 7 shows the percentages of reductions of the story drifts, where it is observed that the lowest reductions happen in the MR-OFF scenario.

According to Figure 7, the MR-ON and CO-LQR scenarios showed good reductions for all stories and the CO-LQR (MR + TMD). It is observed that the optimized hybrid control CO-LQR (MR + MTD) resulted in the highest reductions, at the lowest stories (except on the 1st floor), precisely those that should be controlled. Furthermore, this control scenario was the only one that had effective control over the structure response; therefore, this is the best control scenario for the considered building.

Overall, the proposed methodology, which uses an optimization procedure to determine the optimal TMD parameters and LQR weighting matrices, improved the efficiency of this system and proved to be an excellent tool for designing vibration control systems. Unlike other design methods, such as the authors of [18, 54, 55] which are

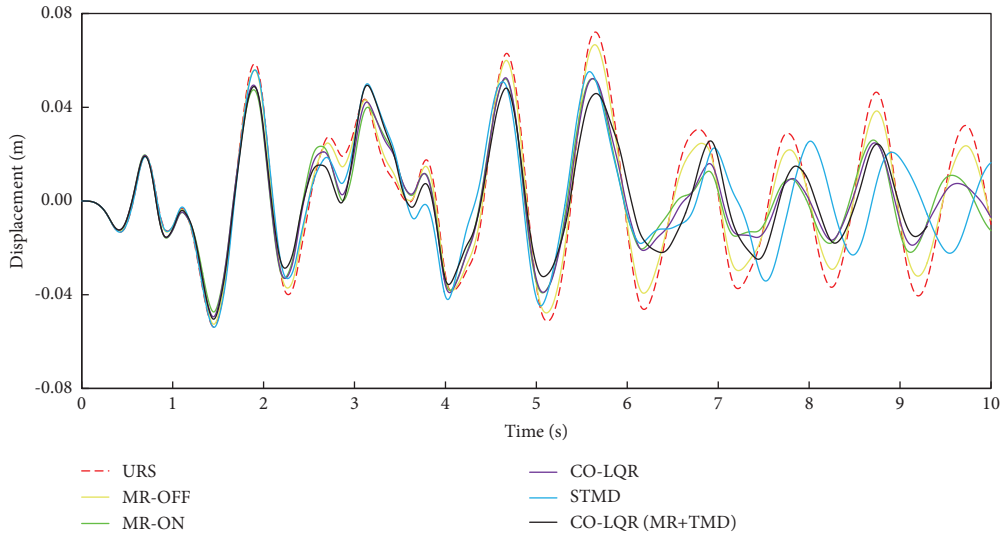

Figure 5: Response in terms of displacements of the 10th story for all control scenarios.

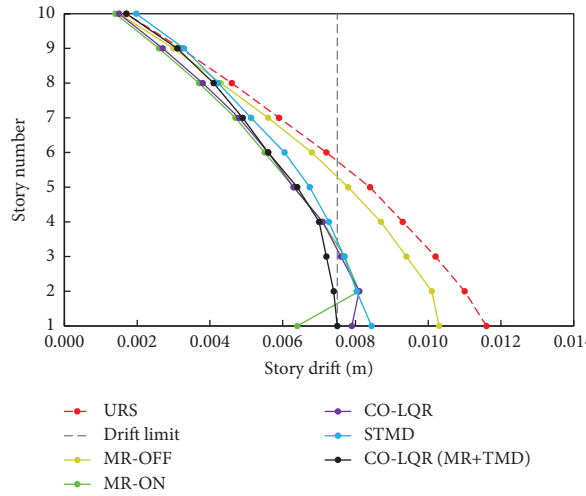

Figure 6: Story drift for uncontrolled and controlled scenarios.

Table 3: Story drift reduction percentages of the analyzed control scenarios.

Story	MR-OFF (%)	MR-ON (%)	CO-LQR (%)	STMD (%)	MR + TMD (%)
1	11.2069	44.8276	31.8966	27.2307	35.3448
2	8.1818	26.3636	26.3636	26.9608	32.7273
3	7.8431	24.5098	25.4902	24.6319	29.4118
4	6.4516	23.6559	23.6559	21.8439	24.7312
5	7.1429	25.0000	25.0000	19.7203	23.8095
6	5.5556	23.6111	22.2222	15.9935	22.2222
7	5.0847	20.3390	18.6441	13.0578	16.9492
8	6.5217	19.5652	17.3913	8.1377	10.8696
9	6.2500	18.7500	15.6250	−2.6264	3.1250
10	11.7647	17.6471	11.7647	−16.4137	0.0000

classical methods used for the design of single TMD, in which the parameters of the device are calculated based on the first modal shape of the structure, the design based on the optimization algorithms, such as meta-heuristics like WOA, calculates the optimal TMD parameters based on an objective function which in the case of this work was the minimization of story drift and associated with a semiactive device generates a hybrid control which is designed for maximum efficiency.

In addition, the optimization procedure by meta-heuristics algorithms has advantages over classical methods, such as they do not require function gradient

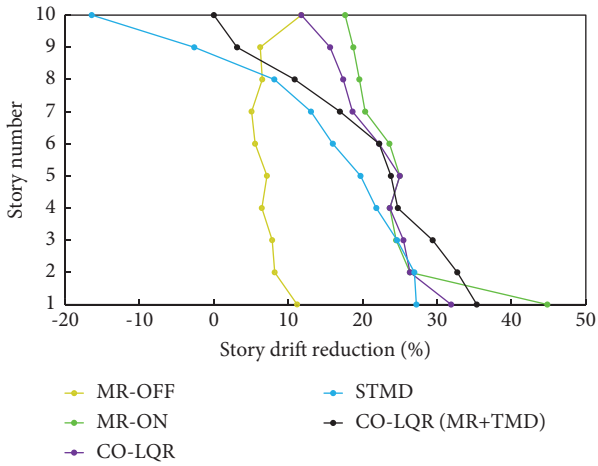

Figure 7: Story drift reductions for all control scenarios.

information; they do not get stuck in local minima, if adjusted correctly; they can be used to solve problems with mixed variables; they can be applied to nonconvex or discontinuous functions; and they provide a set of optimal solutions, so the designer can choose the one that best fits his project. Therefore, the proposed methodology can be a useful tool to assist designers of these types of vibration control systems and contribute to improving the efficiency of the project.

5. Conclusions

The focus of this work was the reduction of the response of buildings subjected to seismic excitation through a hybrid control (MR + TMD) designed using a new methodology that involves the use of metaheuristic optimization. Different control scenarios were proposed and evaluated to determine the best control scenario, in relation to the adopted control criterion. A 10-story shear building was evaluated with a single MR installed between the ground and the first story, operating in passive OFF and ON modes and in semiactive mode with current control by CO-LQR. Furthermore, the response was also evaluated through traditional passive control, with a single TMD installed on the top floor.

The WOA was employed to design the parameters of the TMD (k_{TMD} and c_{TMD}) and LQR for the weight matrices (q_{LQR} and r_{LQR}). Regarding the analyzed scenarios, MR-OFF presented the worst reductions, while in the MR-ON mode, it was verified the highest reduction (44.8276%) at the 1st story. The CO-LQR mode showed good reductions, however, similar to the MR-ON mode. The STMD scenario showed reasonable reductions; however, it generated an increase in the structural response in the last two stories. Nevertheless, it should be noted that the mass of the TMD was taken as just 1% of the total mass of the structure. On the other hand, the MR has a mass of 250 kg, which represents only 7.14% of the mass of the TMD.

Overall, the optimized hybrid control scenario (MR + TMD) shows to be the best alternative to control the response of the building and adapt all story drift to the control criterion. Thus, the proposed methodology can be a useful tool to assist designers of these types of vibration control systems.

Nomenclature

Λ: Location vector of the seismic forces
$\mathbf{A}$: System state matrix
$\mathbf{B_c}$: Vector of the position of the vector control forces, input matrix
$\mathbf{B_{ce}}$: Location matrix of the control forces
$\mathbf{C}$: Output matrix
$\mathbf{C_s}$: Global damping matrix of the structure
$\mathbf{D_c}$: Vector of the position of the vector control forces
$\mathbf{D_{ce}}$: Location matrix of the excitation forces
$\mathbf{E}$: Vector of the location of the seismic acceleration vector
$\mathbf{F}$: Vector of the position of the seismic accelerations
$\mathbf{G}$: Gain matrix
$\mathbf{K_s}$: Global stiffness matrix of the structure
$\mathbf{M_s}$: Global mass matrix of the structure
$\mathbf{P}$: Symmetric matrix, which is the solution of the Riccati equation
$\mathbf{Q}$: Weighting matrices of the LQR controller
$\mathbf{R}$: Weighting matrices of the LQR controller
Γ: Control force location matrix of the control force vector
$\mathbf{f_o}(t)$: Vector of control forces
$\mathbf{f_{mr}}(t)$: Control force vector
$\overrightarrow{\ddot{\mathbf{u}}}_{\mathbf{g}}(t)$: Stationary accelerogram
$\mathbf{x}(t)$: Displacement vector
$\dot{\mathbf{x}}(t)$: Velocity vector
$\dot{\mathbf{x}}_{\mathbf{(2nx1)}}$: Vector of states
$\ddot{\mathbf{x}}(t)$: Acceleration vector
$\ddot{\mathbf{x}}_{\mathbf{g}}(t)$: Seismic acceleration vector
A_{bw}: Parameter of the MBW that describes the hysteresis of the system
a_1: Parameter 1 of the envelope function
a_2: Parameter 2 of the envelope function
α: Parameter of the MBW that describes the hysteresis of the system
β: Parameter of the MBW that describes the hysteresis of the system
c_0: Viscous damping of the MBW observed at larger velocities
c_i: Damping of each story of the building
c_1: Dashpot of the MBW that was included in the model to produce the roll-off that was observed in the experimental data at low velocities
c_{TMD}: Damping of the TMD
d_{i-1}: Maximum displacement of the lower story
d_i: Maximum displacement of the upper story
$\Delta_{h,\max}$: Maximum calculated value for story drift
$\Delta\omega$: Frequency increment
ξ_g: Soil damping
$F = f_{mr}$: Damping force of the MR damper for MBW
f_o: Optimal control force generated by the LQR
$f(\mathbf{g})$: Objective function
$g(t)$: Envelope function
H: Heaviside function

h_i: Height of each story of the building
I_c: MR command current
I_{max}: Maximum current
k_0: Stiffness of the MBW to control stiffness at large velocities
k_1: Accumulator stiffness of the MBW
k_i: Stiffness of each story of the building
k_{TMD}: Stiffness of the TMD
m: Number of MR actuators
m_i: Mass of each story of the building
m_{TMD}: Mass of the TMD
n: Number of degrees of freedom (DOF)
n_{bw}: Parameter of the MBW that describes the hysteresis of the system
N_ω: Interval number of band frequency
$S(\omega)$: Power spectral density (PSD) function
S_0: Constant spectral density
ω_g: Soil frequency
φ_j: Random phase angle, with values uniformly distributed from 0 to 2π
q_{LQR}: LQR factor for **Q** weighting matrix
r_{LQR}: LQR factor for **R** weighting matrix
x_0: Initial displacement of spring k_1 for the MBW
x: Displacement of the controlled structure
$\dot{x}$: Velocity of the controlled structure
$\dot{y}$: Derivative internal displacement of the MBW
γ: Parameter of the MBW that describes the hysteresis of the system
z: Evolutionary variable of the MBW.

Data Availability

The data used to support the findings of this study are available from the corresponding author upon request.

Conflicts of Interest

The authors declare that there are no conflicts of interest.

Acknowledgments

The authors would like to acknowledge the financial support by CAPES and CNPq, Brazil.

References

[1] Brazilian Association of Technical Standards (ABNT), *NBR 15421: Design of Seismic Resistant Structures-Procedure*, ABNT, Rio de Janeiro, 2006.

[2] Ministry of Environment, Housing and Land Development (Mavdt), *Colombian Standard for Seismic-Resistant Structures-NSR-10*, MAVDT, Bogotá, 2010.

[3] AMERICAN INSTITUTE OF STEEL CONSTRUCTION (AISC), *ANSI/AISC 360-16: Specification for Structural Steel Buildings*, AISC, Chicago, Illinois, 2016.

[4] M. D. Symans and M. C. Constantinou, "Semi-active control systems for seismic protection of structures: Semi-active control systems for seismic protection of structures: a state-of-the-art review state-of-the-art review," *Engineering Structures*, vol. 21, no. 6, pp. 469–487, 1999.

[5] T. E. Saaed, G. Nikolakopoulos, J. E. Jonasson, and H. Hedlund, "A state-of-the-art review of structural control systems," *Journal of Vibration and Control*, vol. 21, no. 5, pp. 919–937, 2015.

[6] S. Thenozhi and W. Yu, "Advances in modeling and vibration control of building structures," *Annual Reviews in Control*, vol. 37, no. 2, pp. 346–364, 2013.

[7] M. Bitaraf, S. Hurlebaus, and L. R. Barroso, "Active and semi-active adaptive control for undamaged and damaged building structures under seismic load," *Computer-Aided Civil and Infrastructure Engineering*, vol. 27, no. 1, pp. 48–64, 2011.

[8] M. T. B. César, *Vibration control of building structures using magneto rheological dampers*, Ph.D. Thesis, Ph. D. in Civil Engineering-Faculty of Engineering of the University of Porto, Porto, Portugal, 2015.

[9] M. Bitaraf, *Enhancing the structural performance with active and semi-active devices using adaptive control strategy*, Ph.D. Thesis, (Ph.D. in Civil Engineering)-Texas A&M University, Texas, TX, USA, 2011.

[10] B. F. Spencer, S. R. Nagarajaiah, and S. Nagarajaiah, "State of the State of the Art of Structural Controlrt of structural control," *Journal of Structural Engineering*, vol. 129, no. 7, pp. 845–856, 2003.

[11] F. Weber, H. Distl, F. Feltrin, and M. Motavalli, "Evaluation procedure of decay measurements of a cable with passive-on operating MR damper," in *Proceedings of the Sixth International Symposium on Cable Dynamics*, pp. 143–150, Charleston, CA USA, 2005.

[12] Y. Choi, N. M.-T. Wereley, and N. M. Wereley, "Shock Shock Isolation Systems Using Magnetorheological Damperssolation systems using magnetorheological dampers," *Journal of Vibration and Acoustics*, vol. 130, no. 2, 2008.

[13] D. Simon and M. Ahmadian, "Vehicle Vehicle Evaluation of the Performance of Magneto Rheological Dampers for Heavy Truck Suspensionsvaluation of the performance of Magneto rheological dampers for heavy truck suspensions," *Journal of Vibration and Acoustics*, vol. 123, no. 3, pp. 365–375, 2001.

[14] L. S. Vellar, S. P. Ontiveros-Pérez, L. F. F. Miguel, and L. F. F. Fadel Miguel, "Robust optimum design of multiple tuned mass dampers for vibration control in buildings subjected to seismic excitation," *Shock and Vibration*, vol. 2019, Article ID 9273714, 9 pages, 2019.

[15] Z. Lu, D. Wang, and Y. Zhou, "Experimental parametric study on wind-induced vibration control of particle tuned mass damper on a benchmark high-rise building," *The Structural Design of Tall and Special Buildings*, vol. 26, no. 8, pp. e1359–12, 2017.

[16] S. Elias and V. Matsagar, "Research developments in vibration control of structures using passive tuned mass dampers," *Annual Reviews in Control*, vol. 44, pp. 129–156, 2017.

[17] R. C. Battista and M. S. Pfeil, "Control of wind oscillations of Rio-Niterói bridge, Brazil," *Proceedings of the Institution of Civil Engineers-Structures and Buildings*, vol. 163, no. 2, pp. 87–96, 2010.

[18] J. P. Den Hartog, *Mechanical Vibrations"*, McGraw-Hill, New York, NY, USA, 1956.

[19] M. Mohebbi, K. Shakeri, Y. Ghanbarpour, and H. Majzoub, "Designing optimal multiple tuned mass dampers using genetic algorithms (GAs) for mitigating the seismic response of structures," *Journal of Vibration and Control*, vol. 19, no. 4, pp. 605–625, 2013.

[20] A. Kaveh, S. Mohammadi, O. K. Hosseini, A. Keyhani, and V. R. Kalatjari, "Optimum parameters of tuned mass dampers for seismic applications using charged system search,"

Transactions of Civil Engineering, vol. 39, no. C1, pp. 21–40, 2015.

[21] L. F. Fadel Miguel, R. H. Lopez, L. F. F. Miguel, and A. J. Torii, "A novel approach to the optimum design of MTMDs under seismic excitations," *Structural Control and Health Monitoring*, vol. 23, no. 11, pp. 1290–1313, 2016.

[22] B. B. Rossato and L. F. F. Miguel, "Robust optimum design of tuned mass dampers for high-rise buildings subject to wind-induced vibration," *Numerical Algebra, Control and Optimization*, vol. 13, no. 1, pp. 154–168, 2023.

[23] L. F. F. Miguel and O. A. P. D. Souza, "Robust optimum design of MTMD for control of footbridges subjected to human-induced vibrations via the CIOA," *Structural Engineering & Mechanics*, vol. 86, no. 5, pp. 647–661, 2023.

[24] R. E. Roberson, "Synthesis of a nonlinear dynamic vibration absorber," *Journal of the Franklin Institute*, vol. 254, no. 3, pp. 205–220, 1952.

[25] J. B. Hunt, *Dynamic Vibration Absorbers"*, Mechanical engineering publications, Los Angeles, LA, USA, 1979.

[26] Z. Lu, X. Chen, D. Zhang, and K. Dai, "Experimental and analytical study on the performance of particle tuned mass dampers under seismic excitation," *Earthquake Engineering & Structural Dynamics*, vol. 46, no. 5, pp. 697–714, 2017.

[27] Z. Lu, Z. Wang, Y. Zhou, and X. Lu, "Nonlinear dissipative devices in structural vibration control: Nonlinear dissipative devices in structural vibration control: A review review," *Journal of Sound and Vibration*, vol. 423, pp. 18–49, 2018.

[28] F. Amini and R. Doroudi, "Control of a building complex with Control of a building complex with Magneto-Rheological Dampers and Tuned Mass Damperagneto-rheological dampers and tuned mass damper," *Structural Engineering and Mechanics*, vol. 36, no. 2, pp. 181–195, 2010.

[29] A. Bathaei, S. M. Zahrai, and M. Ramezani, "Semi-active seismic control of an 11-DOF building model with TMD+MR damper using type-1 and-2 fuzzy algorithms," *Journal of Vibration and Control*, vol. 24, no. 13, pp. 2938–2953, 2018.

[30] V. Bhaiya, S. D. Bharti, M. K. Shrimali, and T. K. Datta, "Hybrid seismic control of buildings using tuned mass and magnetorheological dampers," *Proceedings of the Institution of Civil Engineers-Structures and Buildings*, vol. 173, no. 7, pp. 471–487, 2020.

[31] Z. Lu, K. Li, Y. Ouyang, and J. Shan, "Performance-based optimal design of tuned impact damper for seismically excited nonlinear building," *Engineering Structures*, vol. 160, pp. 314–327, 2018.

[32] M. Abdeddaim, S. Djerouni, A. Ounis, B. Athamnia, and E. Noroozinejad Farsangi, "Optimal design of Magneto-rheological damper for seismic response reduction of Base-Isolated structures considering Soil-Structure interaction," *Structures*, vol. 38, pp. 733–752, 2022.

[33] S. H. Hosseini Lavassani, S. Shangapour, P. Homami, V. Gharehbaghi, E. Noroozinejad Farsangi, and T. Y. Yang, "An innovative methodology for hybrid vibration control (MR+TMD) of buildings under seismic excitations," *Soil Dynamics and Earthquake Engineering*, vol. 155, no. 15p, 2022.

[34] K. Kanai, "An empirical formula for the spectrum of Strong earthquake motions," *Bulletin Earthquake Research*, Institute-University of Tokyo, vol. 39, no. 1, pp 85–95, 1961.

[35] H. Tajimi, "A statistical method of determining the maximum response of a building structure during an earthquake," in *Proceedings of the 2nd World Conference in Earthquake Engineering*, pp. 781–797, Tokyo, Japan, 1960.

[36] S. Mirjalili and A. Lewis, "The whale optimization algorithm," *Advances in Engineering Software*, vol. 95, pp. 51–67, 2016.

[37] H. Seya, M. E. Talbott, and H. H. M. Hwang, "Probabilistic seismic analysis of a steel frame structure," *Probabilistic Engineering Mechanics*, vol. 8, no. 2, pp. 127–136, 1993.

[38] M. Shinozuka and C. M. Jan, "Digital simulation of random processes and its applications," *Journal of Sound and Vibration*, vol. 25, no. 1, pp. 111–128, 1972.

[39] T. I. Hsu and M. C. Bernard, "A random process for earthquake simulation," *Earthquake Engineering Earthquake Engineering & Structural Dynamics Structural Dynamics*, vol. 6, no. 4, pp. 347–362, 1978.

[40] J. R. Spencer, S. J. Dyke, M. K. Sain, and J. D. Carlson, "Phenomenological model of a magnetorheological damper," *Journal of Engineering Mechanics*, vol. 123, no. 3, pp. 1–23, 1997.

[41] G. Yang, B. Spencer, J. Carlson, M. F. Sain, J. D. Carlson, and M. K. Sain, "Large-scale MR fluid dampers: modeling and dynamic performance considerations," *Engineering Structures*, vol. 24, no. 3, pp. 309–323, 2002.

[42] S. J. Dyke, *Acceleration feedback control strategies for active and semi-active control systems: modeling, algorithm development, and experimental verification*, (Degree of Doctor of Philosophy)-University of Notre Dame, Ph.D. thesis, 1996.

[43] S. Dyke, M. K. Sain, J. D. R. Carlson, M. K. Sain, and J. D. Carlson, "Modeling and control of magnetorheological dampers for seismic response reduction," *Smart Materials and Structures*, vol. 5, no. 5, pp. 565–575, 1996.

[44] S. J. Dyke, J. R. Spencer, M. K. Sain, and J. D. Carlson, "Seismic response reduction using magnetorheological dampers," in *Proceedings of the 13th Triennial World Congress*, pp. 5530–5535, San Francisco, USA, 1996.

[45] S. Etedali and H. Rakhshani, "Optimum design of tuned mass dampers using multiobjective cuckoo search for buildings under seismic excitations," *Alexandria Engineering Journal*, vol. 57, no. 4, pp. 3205–3218, 2018.

[46] F. D. S. Brandão and L. F. F. Miguel, "Vibration control in buildings under seismic excitation using optimized tuned mass dampers," *Frattura Frattura ed Integrità Strutturaled Integrità Strutturale*, vol. 14, no. 54, pp. 66–87, 2020.

[47] A. Kaveh, T. Bakhshpoori, and M. Azimi, "Seismic optimal design of 3D steel frames using cuckoo search algorithm," *The Structural Design of Tall and Special Buildings*, vol. 24, no. 3, pp. 210–227, 2015.

[48] C. B. Barranco, "Optimization of steel frames and viscous dampers under seismic excitation," *(Master's in Mechanical Engineering)*, Master Thesis, Federal University of Rio Grande do Sul, Porto Alegre, Brazil, 2020.

[49] F. S. Brandão, "Optimization of tuned mass dampers for vibration control in buildings under seismic excitation," *(Master's in Civil Engineering)*, Master Thesis, Federal University of Rio Grande do Sul, Porto Alegre, Brazil, 2021.

[50] F. D. S. Brandão, A. K. de Almeida, and L. F. F. Miguel, "Optimum Optimum Design of Single and Multiple Tuned Mass Dampers for Vibration Control in Buildings Under Seismic Excitationesign of single and multiple tuned mass dampers for vibration control in buildings under seismic excitation," *International Journal of Structural Stability and Dynamics*, vol. 22, no. 08, 2022.

[51] S. P. Ontiveros-Pérez and L. F. F. Miguel, "Reliability-based optimum design of multiple tuned mass dampers for minimization of the probability of failure of buildings under earthquakes," *Structures*, vol. 42, pp. 144–159, 2022.

[52] F. D. S. Brandão and L. F. F. Miguel, "Otimização de parâmetros de projeto de atenuador dinâmico sincronizado (ads) para redução do story drift em edifício," *Revista Mundi Engenharia, Tecnologia e Gestão (ISSN: 2525-4782)*, vol. 6, no. 3, pp. 349–401, 2022.

[53] L. F. F. Miguel and G. P. Santos, "Optimization of multiple tuned mass dampers for road bridges taking into account bridge-vehicle interaction, random pavement roughness, and uncertainties," *Shock and Vibration*, vol. 2021, Article ID 6620427, 9 pages, 2021.

[54] G. B. Warburton and E. O. Ayorinde, "Optimum absorber parameters for simple systems," *Earthquake Engineering Earthquake Engineering & Structural Dynamics Structural Dynamics*, vol. 8, no. 3, pp. 197–217, 1980.

[55] G. B. Warburton, "Optimum absorber parameters for various combinations of response and excitation parameters," *Earthquake Engineering Earthquake Engineering & Structural Dynamics Structural Dynamics*, vol. 10, no. 3, pp. 381–401, 1982.